IEEE Access
Multidisciplinary | Rapid Review | Open Access Journal

Received January 27, 2020, accepted February 4, 2020, date of publication February 10, 2020, date of current version February 19, 2020.

Digital Object Identifier 10.1109/ACCESS.2020.2973044

Robust Dual-Color Watermarking Based on Quaternion Singular Value Decomposition

YONG CHEN[1], ZHIGANG JIA[2], YAN PENG[1], AND YAXIN PENG[3], (Member, IEEE)
[1]School of Mechatronic Engineering and Automation, Shanghai University, Shanghai 200444, China
[2]School of Mathematics and Statistics, Jiangsu Normal University, Xuzhou 221116, China
[3]Department of Mathematics, Shanghai University, Shanghai 200444, China

Corresponding author: Yan Peng (pengyan@shu.edu.cn)

This work was supported in part by the National Natural Science Foundation of China under Grant 61773254, Grant U1813217, Grant 11602133, Grant 91648119, and Grant 11771188, in part by the Basic Research Program of Shanghai Municipal Science and Technology Commission under Grant 16JC1400900, and in part by the Project of Shanghai Municipal Science and Technology Commission under Grant 17DZ1205000.

ABSTRACT This paper proposes a robust dual-color watermarking based on quaternion singular value decomposition (QSVD), which can embed large payloads into color images with low distortion, and can obtain strong robustness to process color image in a holistic manner. First, two notes are proposed for designing the proposed watermarking scheme, one of which is about three strong correlations found in U that can be used for watermark embedding, and the other is analyzing the feasibility of V compensation for QSVD-based watermarking scheme. In addition, a fast structure-preserving algorithm is used to calculate the singular value decomposition (SVD) of a quaternion matrix, which makes the procedure computationally more flexible and efficient. Then a new watermarking scheme is proposed to protect the copyright of color images. This scheme uses quaternion to make the color image channels correlated so that the proposed watermarking scheme has strong anti-attack performance. Experimental results show that the proposed dual-color watermarking is not only imperceptible but also robust to some common attacks, and the performance of the proposed method outperforms other methods considered in this work.

INDEX TERMS QSVD, structure-preserving method, image watermarking, robustness.

I. INTRODUCTION

Today in the era of big data, the rapid development of new information technologies has led to the security and copyright protection in multimedia applications and services becoming an important issue that needs to be solved urgently. Among these existing technologies, the digital watermarking provides a feasible way to protect multimedia data from illegal manipulation and replication. For example, it is very useful in military image processing, remote sensing [1], [2], medical image sharing [3]–[5], multimedia file management, etc.

Many watermarking methods have been well developed [6], [7]. One can use a random sequences number or a recognizable binary pattern or an image as a digital watermark [8]–[10]. As for the carrier, most existing watermarking techniques use a grayscale image [11]–[16] as the host image. In recent years, color image watermarking [17]–[28] has become one of the hot research topics due to the rapid application of color image technology on the Internet. Compared with grayscale image, color image has two advantages: (1) more data can be hidden; (2) higher fidelity can be obtained, the reason is that the color perception depends not only on luminance information but also on chrominance information. The dual-color (i.e., watermark image and host image are color images) image watermarking scheme was studied [19]–[24] to meet the high fidelity and more information hiding. However, color image watermarking is more challenging compared with single channel grayscale image. The following summarizes the typical strategies for color image watermarking in the spatial domain.

A. SINGLE CHANNEL PROCESSING

In this strategy, a binary sequence or grayscale image is usually embedded in a color channel of the host image [17], [18]. This strategy may be flawed because it does not take into account the implication of the Human Visual System. Especially, it is sensitive to color brightness and perception.

The associate editor coordinating the review of this manuscript and approving it for publication was Donatella Darsena.

B. MULTI-CHANNEL PROCESSING

Many existing dual-color watermarking schemes are designed to separate the three channels of color image and mark them in a single channel between the corresponding channels [19]–[24]. Whether single channel processing or multichannel synthesis, its essence is to treat greyscale image, which has some disadvantages: (i) they are sensitive to color attacks because the correlation between different color channels is ignored, (ii) they are not always robust to geometric distortions caused by neglecting the synchronization of color channels.

C. TRIAD CHANNEL PROCESSING

The strategy rearranges three color channels (R, G, B) of the color image into a rectangular matrix as follows

$$M = \left[R^T, G^T, B^T \right]^T,$$

and then marks the real matrix M directly. Obviously, the three channels are processed synchronously in a holistic manner. In [25], based on Arnold scrambling and SVD, Li *et al.* proposed a dual-color watermarking scheme, which has very low computational complexity. This algorithm uses singular values for watermark embedding, which reduces the fidelity of the watermarked image and is fragile for some attacks.

D. QUATERNION PROCESSING

A color image can be represented by a pure quaternion matrix. In this way, color images can be processed holistically without ignoring channel correlation and synchronicity. Wang *et al*. [26] proposed a zero-watermarking algorithm based on quaternion exponential moments (QEM) for resisting geometric attacks on color images. Experimental results show that the algorithm has better resistance to geometric attacks. Later, they developed a new lossless watermarking algorithm using the quaternion discrete Fourier transform (QDFT) [27]. The low sensitivity of the magnitude information obtained by QDFT makes the designed watermarking scheme have better visual quality. Based on quaternion polar harmonic transforms (QPHTs), Xia *et al.* [28] proposed a color medical image lossless watermarking algorithm for copyright protection, which has strong robustness and security. Based on the ternary radial harmonic Fourier moment (TRHFM), Wang *et al.* [29] proposed a quaternion-like stereo image zero-watermarking algorithm. Experimental results show that this new algorithm is robust against various asymmetric and symmetric attacks. At a certain level, various watermarking algorithms combined with quaternion have good visual quality and strong anti-attack ability [30], [31]. These algorithms are very effective and have room for improvement in reducing the computational complexity and increasing the watermark capacity.

In recent years, SVD-based watermarking methods have become one of the research hotspots because of its low complexity and stability [15], [21], [22], [25], [32]–[35]. This stability is that the relationship between the elements in the first column of the U component generated by SVD can be preserved when general image processing is performed. However, this is an embedded watermarking technique that degrades the quality of the original host image. Therefore, the researcher's focus shifts to the fidelity of the watermarked image. Fan *et al.* citeFWL08 considered to modify the elements in the first column of U (V) component for watermarking and adopt the V (U) component to compensate the visible distortion when embedding the watermark into the U (V) component of SVD. This method can reduce the modified quantity, worse case, the number of modified pixels is increased again to N^2 at some time, because at the same time it also changes other pixels that need not to be modified. Su *et al.* [22] further considered the compensation scheme by combining the modified pixels with the original pixels that need not to be modified to compensate for visible distortion. No matter what kind of compensation scheme is adopted, the effect of compensation for visible distortion is not obvious. These compensations affect the original data structure, resulting in the quality of the extracted watermark becomes worse. In fact, the principle of hiding secret information is that it does not affect the normal use of the image, and the watermark can be extracted and used for ownership verification and verification.

In order to overcome these shortcomings, this paper proposes a new robust dual-color watermarking based on QSVD. This scheme meets some requirements, including transparency, robustness, sufficient information capacity, low computational complexity, and blind extraction. Two notes are presented for designing the proposed watermarking scheme, one of which is about three strong correlations found in U that can be used for watermark embedding, and the other is analyzing the feasibility of V compensation for QSVD-based watermarking scheme. In order to avoid more operations of the QSVD algorithm, we use a fast algebraic structure-preserving method to implement the SVD of the pure quaternion matrix. The experimental results verify the impact of the compensation scheme on the quality of the extracted watermark. It also shows that the proposed watermarking method with two notes is effective and has better performance than the other methods considered in this paper. The novelties of this scheme are as follows: (1) three strong correlations are found in U that can be used to embed ternary watermark information simultaneously, which improves the payload of the proposed watermarking scheme; (2) the feasibility of V compensation is analyzed for (Q)SVD-based watermarking schemes; (3) the structure-preserving algorithm introduced in this paper can quickly and efficiently calculate the SVD of a quaternion matrix; (4) the proposed dual-color watermarking scheme based on QSVD can effectively resist geometric attacks and common attacks; and (5) this scheme has high security because it is based on two private keys of Arnold scrambling and random coordinate sequences.

The remainder of this paper is organized as follows. In Section II, quaternion and algebraic structure-preserving algorithms for implementing QSVD are briefly introduced. Two notes are presented for the QSVD-based watermarking scheme in Section III. In Section IV, a new watermarking scheme is described, including watermark embedding and watermark extraction. The experimental results and analysis are presented in Section V. Finally, we draw the conclusions of this paper in Section VI.

II. PRELIMINARIES

The quaternion, which is a type of hypercomplex number, was formally introduced by Hamilton in 1843 [36]. A quaternion can be represented as a four-dimensional complex number with one real part and three imaginary parts. The set of quaternions is denoted by

$$\mathbb{H} = \{q = w + x\mathbf{i} + y\mathbf{j} + z\mathbf{k}, \quad w, x, y, z \in \mathbb{R}\},$$

where three imaginary units $\mathbf{i}, \mathbf{j}, \mathbf{k}$ satisfy $\mathbf{i}^2 = \mathbf{j}^2 = \mathbf{k}^2 = -1$, $\mathbf{ij} = -\mathbf{ji} = \mathbf{k}$, $\mathbf{jk} = -\mathbf{kj} = \mathbf{i}$, $\mathbf{ki} = -\mathbf{ik} = \mathbf{j}$. When $w = 0$, q is called pure quaternion.

Color image pixels have three components, and they can be represented in quaternion form using pure quaternion. A pixel coordinate (x, y) in an RGB image H can be represented as

$$H(x, y) = H_1(x, y)\mathbf{i} + H_2(x, y)\mathbf{j} + H_3(x, y)\mathbf{k},$$

where H_1, H_2 and H_3 are the red, green and blue components, respectively. Obviously, the advantage of using quaternion to represent color image is that we can process the three color channels of a color image holistically without losing correlation and synchronicity.

A. ALGEBRAIC STRUCTURE-PRESERVING ALGORITHM FOR QSVD

Suppose $H \in \mathbb{H}^{m\times n}$ is a quaternion matrix, then there exist two unitary quaternion matrices $U = U_0 + U_1\mathbf{i} + U_2\mathbf{j} + U_3\mathbf{k} \in \mathbb{H}^{m\times m}$ and $V = V_0 + V_1\mathbf{i} + V_2\mathbf{j} + V_3\mathbf{k} \in \mathbb{H}^{n\times n}$ such that [37]

$$H = U\Sigma V^*, \Sigma = \begin{bmatrix} \Sigma_1 & 0 \\ 0 & 0 \end{bmatrix}, \tag{II.1}$$

where $V^* = V_0^T - V_1^T\mathbf{i} - V_2^T\mathbf{j} - V_3^T\mathbf{k}$ is the conjugate transpose of V, $\Sigma_1 = diag(\sigma_1, \sigma_2, \cdots, \sigma_r)$, $\sigma_1 \geq \sigma_2 \geq \cdots \geq \sigma_r > 0$ are positive singular values of Q, and r is the rank of matrix Q.

For a color image represented by a pure quaternion matrix $H \in \mathbb{H}^{m\times n}$, we can perform the QSVD with different kinds of algorithms. For example, Sangwine and Le Bihan [38] provided the function `svd` in Matlab Toolbox using quaternion arithmetics. In [39], Jia *et al.* proposed a real structure-preserving algorithm based on the following results.

For any quaternion matrix $H = H_0 + H_1\mathbf{i} + H_2\mathbf{j} + H_3\mathbf{k}$, where $H_0, H_1, H_2, H_3 \in \mathbb{R}^{m\times n}$, its real counterpart can be defined as follows:

$$H^R \equiv \begin{bmatrix} H_0 & H_2 & H_1 & H_3 \\ -H_2 & H_0 & H_3 & -H_1 \\ -H_1 & -H_3 & H_0 & H_2 \\ -H_3 & H_1 & -H_2 & H_0 \end{bmatrix}, \tag{II.2}$$

and their relationship is equivalent. The algebraic structure of H^R is called JRS-symmetry, which is implicitly preserved in the algebraic structure-preserving algorithms used in [39]–[44] to solve many quaternion matrix problems.

In this paper, a hybrid structure-preserving algorithm is proposed for 4×4 quaternion matrix block, which combines the JRSGivens transformation G proposed in [39], the generalized Givens transformation $\mathscr{G}$ proposed in [40], and the Householder transformation $\mathscr{H}$ proposed in [41]. Its calculation process can be summarized into the following algorithm.

Algorithm 1 (QSVD): A structure-preserving method for the computation of the singular values and corresponding singular vectors of a quaternion matrix $H = H_0 + H_1\mathbf{i} + H_2\mathbf{j} + H_3\mathbf{k} \in \mathbb{H}^{m\times n}$, *where* $H_k \in \mathbb{R}^{m\times n}$, $k = 0, 1, 2, 3$.

Function: $[U, \Sigma, V] = \mathtt{QSVD}(H_0, H_1, H_2, H_3)$

1. Calculate the real upper bidiagonal matrix B using unitary quaternion matrices G, $\mathscr{G}$ *and* $\mathscr{H}$*:*

$$B = \begin{bmatrix} I_3 & 0 \\ 0 & G \end{bmatrix}\begin{bmatrix} I_2 & 0 \\ 0 & \mathscr{G} \end{bmatrix}\begin{bmatrix} 1 & 0 \\ 0 & \mathscr{H} \end{bmatrix}\mathscr{H}H\begin{bmatrix} 1 & 0 \\ 0 & \mathscr{H} \end{bmatrix}\begin{bmatrix} I_2 & 0 \\ 0 & \mathscr{G} \end{bmatrix}\begin{bmatrix} I_3 & 0 \\ 0 & G \end{bmatrix}; \tag{II.3}$$

2. Calculate the singular values and corresponding singular vectors of B using MATLAB's built-in function `svd`*:*

$$[u, \lambda, v^T] = \mathtt{svd}(B);$$

3. Compute the singular values and corresponding singular vectors of H:

$$\Sigma = \lambda,$$
$$U = (u^T\begin{bmatrix} I_3 & 0 \\ 0 & G \end{bmatrix}\begin{bmatrix} I_2 & 0 \\ 0 & \mathscr{G} \end{bmatrix}\begin{bmatrix} 1 & 0 \\ 0 & \mathscr{H} \end{bmatrix}\mathscr{H})^*,$$
$$V = \begin{bmatrix} 1 & 0 \\ 0 & \mathscr{H} \end{bmatrix}\begin{bmatrix} I_2 & 0 \\ 0 & \mathscr{G} \end{bmatrix}\begin{bmatrix} I_3 & 0 \\ 0 & G \end{bmatrix}v.$$

The JRS-symmetric structure is preserved throughout the implementation of (II.3). Algorithm 1 costs about $64(mn^2 - n^3/3)$ flops for the bidiagonalization of an $m \times n$ quaternion matrix. For a 512×512 color image divided into 4×4 matrix blocks, two methods can be used to calculate the QSVDs of these image blocks: the proposed QSVD algorithm and the quaternion toolbox. The comparison results of the execution time of the two algorithms are shown in Table 1. Compared with the quaternion toolbox, it can be seen that the efficiency of the proposed QSVD algorithm has been greatly improved.

TABLE 1. The comparison of execution times (second).

Image block (size)/(number)	Proposed method	Quaternion toolbox
$(4 \times 4)/(128 \times 128)$	4.57484	81.12152

III. OUR PROPOSED NOTES

A. SELECTION OF WATERMARK EMBEDDING POSITION

Suppose that a 4×4 reversible quaternion matrix H_s is one of the blocks of the host image, and has the quaternion SVD as

$$H_s = \begin{bmatrix} h_{11} & h_{12} & h_{13} & h_{14} \\ h_{21} & h_{22} & h_{23} & h_{24} \\ h_{31} & h_{32} & h_{33} & h_{34} \\ h_{41} & h_{42} & h_{43} & h_{44} \end{bmatrix} := U\Sigma V^* = \begin{bmatrix} u_{11} & u_{12} & u_{13} & u_{14} \\ u_{21} & u_{22} & u_{23} & u_{24} \\ u_{31} & u_{32} & u_{33} & u_{34} \\ u_{41} & u_{42} & u_{43} & u_{44} \end{bmatrix} \begin{bmatrix} \sigma_1 & 0 & 0 & 0 \\ 0 & \sigma_2 & 0 & 0 \\ 0 & 0 & \sigma_3 & 0 \\ 0 & 0 & 0 & \sigma_4 \end{bmatrix} \begin{bmatrix} v_{11} & v_{12} & v_{13} & v_{14} \\ v_{21} & v_{22} & v_{23} & v_{24} \\ v_{31} & v_{32} & v_{33} & v_{34} \\ v_{41} & v_{42} & v_{43} & v_{44} \end{bmatrix}. \tag{III-1}$$

Perform the matrix multiplications for $U\Sigma V^*$, in which each element is given by (III-2).

$$\begin{aligned}
h_{11} &= u_{11}\sigma_1 v_{11} + u_{12}\sigma_2 v_{21} + u_{13}\sigma_3 v_{31} + u_{14}\sigma_4 v_{41};\\
h_{12} &= u_{11}\sigma_1 v_{12} + u_{12}\sigma_2 v_{22} + u_{13}\sigma_3 v_{32} + u_{14}\sigma_4 v_{42};\\
h_{13} &= u_{11}\sigma_1 v_{13} + u_{12}\sigma_2 v_{23} + u_{13}\sigma_3 v_{33} + u_{14}\sigma_4 v_{43};\\
h_{14} &= u_{11}\sigma_1 v_{14} + u_{12}\sigma_2 v_{24} + u_{13}\sigma_3 v_{34} + u_{14}\sigma_4 v_{44};\\
h_{21} &= u_{21}\sigma_1 v_{11} + u_{22}\sigma_2 v_{21} + u_{23}\sigma_3 v_{31} + u_{24}\sigma_4 v_{41};\\
h_{22} &= u_{21}\sigma_1 v_{12} + u_{22}\sigma_2 v_{22} + u_{23}\sigma_3 v_{32} + u_{24}\sigma_4 v_{42};\\
h_{23} &= u_{21}\sigma_1 v_{13} + u_{22}\sigma_2 v_{23} + u_{23}\sigma_3 v_{33} + u_{24}\sigma_4 v_{43};\\
h_{24} &= u_{21}\sigma_1 v_{14} + u_{22}\sigma_2 v_{24} + u_{23}\sigma_3 v_{34} + u_{24}\sigma_4 v_{44};\\
h_{31} &= u_{31}\sigma_1 v_{11} + u_{32}\sigma_2 v_{21} + u_{33}\sigma_3 v_{31} + u_{34}\sigma_4 v_{41};\\
h_{32} &= u_{31}\sigma_1 v_{12} + u_{32}\sigma_2 v_{22} + u_{33}\sigma_3 v_{32} + u_{34}\sigma_4 v_{42};\\
h_{33} &= u_{31}\sigma_1 v_{13} + u_{32}\sigma_2 v_{23} + u_{33}\sigma_3 v_{33} + u_{34}\sigma_4 v_{43};\\
h_{34} &= u_{31}\sigma_1 v_{14} + u_{32}\sigma_2 v_{24} + u_{33}\sigma_3 v_{34} + u_{34}\sigma_4 v_{44};\\
h_{41} &= u_{41}\sigma_1 v_{11} + u_{42}\sigma_2 v_{21} + u_{43}\sigma_3 v_{31} + u_{44}\sigma_4 v_{41};\\
h_{42} &= u_{41}\sigma_1 v_{12} + u_{42}\sigma_2 v_{22} + u_{43}\sigma_3 v_{32} + u_{44}\sigma_4 v_{42};\\
h_{43} &= u_{41}\sigma_1 v_{13} + u_{42}\sigma_2 v_{23} + u_{43}\sigma_3 v_{33} + u_{44}\sigma_4 v_{43};\\
h_{44} &= u_{41}\sigma_1 v_{14} + u_{42}\sigma_2 v_{24} + u_{43}\sigma_3 v_{34} + u_{44}\sigma_4 v_{44}.
\end{aligned} \tag{III-2}$$

According to the above formulas, each pixel value in H_s depends on the singular values $\sigma_j (1 \le j \le 4)$. The more the modified number for all σ_j is, the bigger the changed magnitude in pixel values is, and the worse the invisibility of the watermark is. This is the main reason why we do not consider using singular values for marking.

Now we are likely to consider that all the column vectors of U (V) component could be adopted for robust watermarking. For example, a pure quaternion matrix $H = H_1\mathbf{i} + H_2\mathbf{j} + H_3\mathbf{k} \in \mathbb{H}^{4\times 4}$ obtained from a digital image block, where

$$H_1 = \begin{bmatrix} 0.2863 & 0.2863 & 0.2863 & 0.2863 \\ 0.1843 & 0.2863 & 0.2863 & 0.2863 \\ 0.1843 & 0.2510 & 0.2863 & 0.3216 \\ 0.2275 & 0.1137 & 0.1843 & 0.2196 \end{bmatrix},$$

$$H_2 = \begin{bmatrix} 0.3569 & 0.3569 & 0.3569 & 0.3569 \\ 0.2235 & 0.3216 & 0.3216 & 0.3216 \\ 0.2196 & 0.3216 & 0.3216 & 0.3216 \\ 0.2196 & 0.1843 & 0.2196 & 0.2510 \end{bmatrix},$$

$$H_3 = \begin{bmatrix} 0.3569 & 0.3569 & 0.3569 & 0.3569 \\ 0.1843 & 0.3216 & 0.3216 & 0.3216 \\ 0.2196 & 0.3059 & 0.3216 & 0.3216 \\ 0.1137 & 0.1804 & 0.2196 & 0.2196 \end{bmatrix},$$

by performing Algorithm 1, we have

$$\begin{aligned}
U &= U_0 + U_1\mathbf{i} + U_2\mathbf{j} + U_3\mathbf{k}\\
&= \begin{bmatrix} -0.0001 & 0.0099 & 0.0792 & -0.0488 \\ 0.0008 & 0.0141 & 0.0757 & -0.0485 \\ 0.0008 & -0.0169 & -0.1632 & 0.1217 \\ -0.0001 & 0.0028 & 0.0240 & -0.0175 \end{bmatrix}\\
&\quad + \begin{bmatrix} -0.3051 & 0.1684 & -0.4715 & 0.0472 \\ -0.2817 & -0.3104 & -0.1079 & 0.4149 \\ -0.2822 & -0.2595 & 0.3133 & -0.5907 \\ -0.1962 & 0.4878 & 0.5018 & 0.1949 \end{bmatrix}\mathbf{i}\\
&\quad + \begin{bmatrix} -0.3762 & 0.2871 & -0.1541 & -0.1202 \\ -0.3175 & -0.2089 & 0.1963 & 0.2530 \\ -0.3168 & -0.2548 & 0.0087 & -0.3152 \\ -0.2311 & 0.1818 & -0.0711 & 0.3085 \end{bmatrix}\mathbf{j}\\
&\quad + \begin{bmatrix} -0.3465 & 0.4518 & -0.0735 & -0.2312 \\ -0.2815 & -0.2448 & 0.3950 & 0.3000 \\ -0.2854 & -0.1014 & -0.0734 & -0.0487 \\ -0.1805 & -0.2665 & -0.3777 & 0.0011 \end{bmatrix}\mathbf{k},\\
V^* &= V_0^T - V_1^T\mathbf{i} - V_2^T\mathbf{j} - V_3^T\mathbf{k}\\
&= \begin{bmatrix} -0.4228 & -0.5031 & -0.5255 & -0.5380 \\ 0.8684 & -0.3310 & -0.2226 & -0.1467 \\ -0.2580 & -0.2813 & 0.0755 & 0.4135 \\ -0.0245 & -0.0876 & 0.3820 & -0.2720 \end{bmatrix}\\
&\quad + \begin{bmatrix} 0 & 0.0186 & 0.0226 & 0.0197 \\ 0 & 0.0749 & 0.0036 & -0.0453 \\ 0 & 0.2004 & 0.0126 & -0.2010 \\ 0 & 0.2225 & -0.3950 & 0.1715 \end{bmatrix}\mathbf{i}\\
&\quad + \begin{bmatrix} 0 & -0.0251 & -0.0196 & -0.0111 \\ 0 & -0.1738 & 0.0332 & 0.1053 \\ 0 & -0.5444 & 0.1521 & 0.3645 \\ 0 & 0.0051 & -0.0882 & 0.0843 \end{bmatrix}\mathbf{j}\\
&\quad + \begin{bmatrix} 0 & 0.0116 & 0.0010 & -0.0058 \\ 0 & 0.0872 & 0.0126 & -0.0860 \\ 0 & 0.2923 & -0.0140 & -0.2427 \\ 0 & -0.1857 & 0.5772 & -0.3928 \end{bmatrix}\mathbf{k},\\
\Sigma &= \begin{bmatrix} 1.9401 & 0 & 0 & 0 \\ 0 & 0.1814 & 0 & 0 \\ 0 & 0 & 0.0785 & 0 \\ 0 & 0 & 0 & 0.0066 \end{bmatrix},
\end{aligned} \tag{III-3}$$

and the accuracy of process is $2.7081e^{-15}$(equal to norm (Q-$U\Sigma V^*$), where $U, V \in \mathbb{H}^{4\times 4}$).

The symbol and magnitude relationship between elements in each column of U (V^*) component obtained by QSVD have been shown (III-3). It is found that the first column ele-

TABLE 2. The NC values of different elements in first column of U component after quaternion SVD.

	Image	NC(u_{11}, u_{21})	NC(u_{11}, u_{31})	NC(u_{11}, u_{41})	NC(u_{21}, u_{31})	NC(u_{21}, u_{41})	NC(u_{31}, u_{41})
i	Peppers	0.9966	0.9931	0.9876	0.9972	0.9925	0.9963
	House	0.9942	0.9860	0.9802	0.9953	0.9877	0.9957
	Baboon	0.9856	0.9775	0.9703	0.9866	0.9727	0.9814
	Monolake	0.9873	0.9772	0.9707	0.9866	0.9769	0.9860
	Safari10	0.9918	0.9742	0.9563	0.9920	0.9727	0.9910
	Redrock2	0.9855	0.9735	0.9643	0.9852	0.9725	0.9840
	Average	0.9902	0.9802	0.9716	**0.9905**	0.9792	0.9891
j	Peppers	0.9906	0.9820	0.9711	0.9952	0.9854	0.9944
	House	0.9946	0.9867	0.9759	0.9953	0.9834	0.9910
	Baboon	0.9772	0.9645	0.9559	0.9786	0.9590	0.9726
	Monolake	0.9926	0.9864	0.9827	0.9922	0.9864	0.9920
	Safari10	0.9956	0.9859	0.9756	0.9957	0.9850	0.9951
	Redrock2	0.9799	0.9650	0.9546	0.9799	0.9642	0.9784
	Average	0.9884	0.9784	0.9693	**0.9895**	0.9772	0.9873
k	Peppers	0.9837	0.9753	0.9632	0.9927	0.9821	0.9914
	House	0.9946	0.9859	0.9724	0.9956	0.9817	0.9900
	Baboon	0.9772	0.9616	0.9509	0.9779	0.9560	0.9734
	Monolake	0.9941	0.9896	0.9871	0.9937	0.9897	0.9937
	Safari10	0.9926	0.9766	0.9601	0.9929	0.9755	0.9920
	Redrock2	0.9849	0.9755	0.9694	0.9852	0.9749	0.9839
	Average	0.9879	0.9774	0.9672	**0.9897**	0.9767	0.9874
Total average		0.9888	0.9787	0.9694	0.9899	0.9777	0.9879

ments of each coefficient matrix (U_1, U_2, U_3) corresponding to the three imaginary parts (**i**, **j**, **k**) have the same sign and their values are very close. This feature can be used to embed watermarks.

In order to select the three best hidden positions among the coefficients of the three imaginary parts of u_{11}, u_{21}, u_{31} and u_{41}, for six standard 512×512 sized color images Peppers, House, Baboon, Monolake, Safari10 and Redrock2 [45], we adopt the following step to experiments.

Step 1: The test image of size $M \times N$ is divided into image blocks of size 4×4.

Step 2: Each image block is decomposed by QSVD to obtain a quaternion matrix U.

Step 3: Matrix $U_x^{\mathbf{i}}$ is composed of the coefficients of the imaginary part i of u_{x1} obtained for each image block, and $U_x^{\mathbf{j}}$ and $U_x^{\mathbf{k}}$ are also the same, where the dimensions of $U_x^{\mathbf{i}}$, $U_x^{\mathbf{j}}$ and $U_x^{\mathbf{k}}$ are $\frac{M}{4} \times \frac{N}{4}$, and $x = 1, 2, 3, 4$, respectively.

Step 4: Calculate the correlation between two matrices $U_x^{\mathbf{i}}$ and $U_y^{\mathbf{i}}$ (between $U_x^{\mathbf{j}}$ and $U_y^{\mathbf{j}}$, between $U_x^{\mathbf{k}}$ and $U_y^{\mathbf{k}}$) using Normalized Cross-Correlation (NC), where $y = 1, 2, 3, 4, x \neq y$.

As can be seen from the Table 2, the average value of the imaginary part **i** of the NC(u_{21}, u_{31}) is 0.9905, the average value of the imaginary part **j** is 0.9895, and the average value of the imaginary part **k** is 0.9897. It indicates that the second row element and the third row element are the closest elements in the first column of each coefficient matrix (U_1, U_2, U_3) for many standard images. Therefore, it is noted that there exists a strong correlation between the second row element and the third row element of the first column of each coefficient matrix (U_1, U_2, U_3).

Summarizing the above analysis and a large number of repetitive experimental results, we give our first proposed note depicted as the following:

Note 1: For the watermarking scheme of 4×4 image block, only the coefficients of the three imaginary parts (**i**, **j**, **k**) of the first column of the U component obtained by QSVD can be modified. Secondly, there is a strong correlation between the second row element and the third row element in the first column of each coefficient matrix (U_1, U_2, U_3).

B. FEASIBILITY OF COMPENSATION METHOD FOR QSVD

According to the three best hidden positions proposed in **Note 1**, we modify u_{21} and u_{31} by $\Delta_1 = \delta_{11}\mathbf{i} + \delta_{12}\mathbf{j} + \delta_{13}\mathbf{k}$ and $\Delta_2 = \delta_{21}\mathbf{i} + \delta_{22}\mathbf{j} + \delta_{23}\mathbf{k}$, respectively, using the watermarking scheme described in Section IV, where δ_{ij} $(i = 1, 2; j = 1, 2, 3)$ is a constant. Thus the elements $h_{ij} (i = 2, 3; j = 1, 2, 3, 4)$ are modified to $\widehat{h}_{ij}$ in the quaternion matrix H_s, as shown in the following formula:

$$
\begin{aligned}
\widehat{h}_{21} &= (u_{21} + \Delta_1)\sigma_1 v_{11} + u_{22}\sigma_2 v_{21} + u_{23}\sigma_3 v_{31} + u_{24}\sigma_4 v_{41};\\
\widehat{h}_{22} &= (u_{21} + \Delta_1)\sigma_1 v_{12} + u_{22}\sigma_2 v_{22} + u_{23}\sigma_3 v_{32} + u_{24}\sigma_4 v_{42};\\
\widehat{h}_{23} &= (u_{21} + \Delta_1)\sigma_1 v_{13} + u_{22}\sigma_2 v_{23} + u_{23}\sigma_3 v_{33} + u_{24}\sigma_4 v_{43};\\
\widehat{h}_{24} &= (u_{21} + \Delta_1)\sigma_1 v_{14} + u_{22}\sigma_2 v_{24} + u_{23}\sigma_3 v_{34} + u_{24}\sigma_4 v_{44};\\
\widehat{h}_{31} &= (u_{31} + \Delta_2)\sigma_1 v_{11} + u_{32}\sigma_2 v_{21} + u_{33}\sigma_3 v_{31} + u_{34}\sigma_4 v_{41};\\
\widehat{h}_{32} &= (u_{31} + \Delta_2)\sigma_1 v_{12} + u_{32}\sigma_2 v_{22} + u_{33}\sigma_3 v_{32} + u_{34}\sigma_4 v_{42};\\
\widehat{h}_{33} &= (u_{31} + \Delta_2)\sigma_1 v_{13} + u_{32}\sigma_2 v_{23} + u_{33}\sigma_3 v_{33} + u_{34}\sigma_4 v_{43};\\
\widehat{h}_{34} &= (u_{31} + \Delta_2)\sigma_1 v_{14} + u_{32}\sigma_2 v_{24} + u_{33}\sigma_3 v_{34} + u_{34}\sigma_4 v_{44}.
\end{aligned}
\tag{III-4}
$$

The specific result of $\widehat{h}_{21}$ is as follows:

$$\begin{aligned}
&\widehat{h}_{21}\\
&= (u_{21}+\Delta_1)\sigma_1 v_{11} + u_{22}\sigma_2 v_{21} + u_{23}\sigma_3 v_{31} + u_{24}\sigma_4 v_{41}\\
&= [\alpha_0 + (\alpha_1+\delta_{11})\mathbf{i} + (\alpha_2+\delta_{12})\mathbf{j}\\
&\quad +(\alpha_3+\delta_{13})\mathbf{k}]\sigma_1(\beta_0+\beta_1\mathbf{i}+\beta_2\mathbf{j}+\beta_3\mathbf{k})\\
&\quad +u_{22}\sigma_2 v_{21} + u_{23}\sigma_3 v_{31} + u_{24}\sigma_4 v_{41}\\
&= \sigma_1[\alpha_0\beta_0 - (\alpha_1+\delta_{11})\beta_1 - (\alpha_2+\delta_{12})\beta_2 - (\alpha_3+\delta_{13})\beta_3]\\
&\quad +\sigma_1[\alpha_0\beta_1 + (\alpha_1+\delta_{11})\beta_0 + (\alpha_2+\delta_{12})\beta_3 - (\alpha_3+\delta_{13})\beta_2]\mathbf{i}\\
&\quad +\sigma_1[\alpha_0\beta_2 + (\alpha_2+\delta_{12})\beta_0 + (\alpha_3+\delta_{13})\beta_1 - (\alpha_1+\delta_{11})\beta_3]\mathbf{j}\\
&\quad +\sigma_1[\alpha_0\beta_3 + (\alpha_3+\delta_{13})\beta_0 + (\alpha_1+\delta_{11})\beta_2 - (\alpha_2+\delta_{12})\beta_1]\mathbf{k}\\
&\quad +u_{22}\sigma_2 v_{21} + u_{23}\sigma_3 v_{31} + u_{24}\sigma_4 v_{41}, \qquad \text{(III-5)}
\end{aligned}$$

where $u_{21} = \alpha_0+\alpha_1\mathbf{i}+\alpha_2\mathbf{j}+\alpha_3\mathbf{k}$, $v_{11} = \beta_0+\beta_1\mathbf{i}+\beta_2\mathbf{j}+\beta_3\mathbf{k}$, and the singular value $\sigma_i (i = 1, 2, 3, 4)$ is a positive real number. As shown in (III-3), the first column element of V^* is a real number rather than a quaternion, which indicates that the values of the coefficients β_1, β_2 and β_3 of the three imaginary parts of v_{11} are zero, so the value of the real part of $\widehat{h}_{21}$ is zero. Similarly, the value of the real part of $\widehat{h}_{31}$ is also zero, but the real part of the remaining six values $\widehat{h}_{ij} (i = 2, 3; j = 2, 3, 4)$ is not zero because the $v_{1j} (j = 2, 3, 4)$ is a quaternion. Fortunately, the real part of these six values is only slightly disturbed and can be ignored.

As shown in (III-4), modifying the values of u_{21} and u_{31} will change the values of $h_{ij} (i = 2, 3; j = 1, 2, 3, 4)$, which inevitably decreases the invisibility of the watermark. Now we can consider the QSVD-based compensation scheme. Recalling the SVD-based compensation scheme proposed in [15] and [22], we can modify some elements of V so that the reconstructed pixel $\widehat{h}_{ij}$ is close to the original pixel $h_{ij} (i = 2, 3; j = 1, 2, 3, 4)$, which an effective compensation scheme to enhance the invisibility of watermark. However, after many experiments, we found that the compensation method has a small improvement in the invisibility of the watermark. On the contrary, this compensation method is tantamount to another attack on the watermarked image, which directly destroys the data structure of the watermarked image and may reduce the quality of the extracted watermark. Specific experimental comparisons are verified in Section V. Similarly, it can be seen from (III-5) that a QSVD-based watermarking scheme with V compensation will severely destroy the real part of the reconstructed quaternion matrix, which not only reduces the invisibility of the watermark but also makes the quality of the extracted watermark worse. Therefore, the real part of the quaternion matrix needs to be as zero as possible without considering the V compensation in this paper.

Summarizing the analysis of the QSVD-based compensation scheme, we give the second proposed note depicted as the following:

Note 2: In the QSVD-based watermarking scheme, the compensation of V is dangerous. If the elements of the first row of V^* are real numbers rather than a quaternions, then the real part of the reconstructed quaternion matrix is a zero matrix.

IV. A NEW COLOR IMAGE WATERMARKING SCHEME

In this section, a QSVD-based watermarking scheme, which explores the property of the U component mentioned in Section III, is proposed to embed a color image watermark as copyright message into a color host image.

A. WATERMARK EMBEDDING

Suppose the original host color image is represented by the pure quaternion matrix $H \in \mathbb{H}^{m\times n}$, and the original color watermark image $W \in \mathbb{H}^{e\times f}$. Now we present the watermark embedding process, which is illustrated by Fig.1, and its detail are listed as follow.

Step 1: Preprocessing of color image watermark W. The original color watermark image is divided into three components of R, G, and B, which are W_R, W_G, and W_B, respectively. In order to improve the security of the watermarking scheme, each component watermark is scrambled by Arnold scrambling with the private key `Ka` and converted from a decimal format to a binary sequence. The watermark sequence $\begin{bmatrix} W_R : \omega_1, \omega_2, \cdots, \omega_p \\ W_G : \omega_1, \omega_2, \cdots, \omega_p \\ W_B : \omega_1, \omega_2, \cdots, \omega_p \end{bmatrix}$ are obtained and $\omega_p \in \{1, 0\}$.

Arnold scrambling is widely used for image scrambling. For the security of the watermarking scheme, even if the infringer obtains the watermarked image, they can not extract the watermark without knowing the scrambling algorithm. The scrambling process is as follows:

$$\begin{bmatrix}\tilde{x}\\ \tilde{y}\end{bmatrix} = \begin{bmatrix}a & b\\ c & d\end{bmatrix}\begin{bmatrix}x\\ y\end{bmatrix} (mod N) \qquad \text{(IV-1)}$$

where a, b, c and d are any positive integers, and $ad - bc = \pm 1$. In this paper, we let $a = b = c = 1, d = 2$. $\tilde{x}$, $\tilde{y}$, x and y are integers in $0, 1, 2, \ldots, N-1$ and N is order of watermark image matrix. The position (x, y) of watermark image pixel can be changed to another position $(\tilde{x}, \tilde{y})$ by (IV-1).

Step 2: The host image is divided into the non-overlapping quaternion matrix blocks H_s of size 4×4 in a holistic way. In order to improve the watermark robustness against cropping attack of the proposed method, the embedded blocks are selected by the random coordinate sequence based on the private key `Kb`.

Step 3: Performing Algorithm 1 on each block H_s as (IV-2) to obtain the matrices U_s, V_s and Σ_s of each block

$$[U_s, \Sigma_s, V_s] = \mathtt{QSVD}(H_s). \qquad \text{(IV-2)}$$

Step 4: According to the watermark information to modify the elements of u_{21} and u_{31} in the quaternion matrix U_s of each embedded block. The watermark is embedded by changing the relation between the second element $(u_{21})_{\mathbf{i/j/k}}$ and the third element $(u_{31})_{\mathbf{i/j/k}}$ in the first column of U_s. If the embedded binary watermark bit is 1, the value of $(u_{21} - u_{31})_{\mathbf{i/j/k}}$ should be negative and its magnitude is greater than a threshold T. If the embedded binary watermark bit is 0,

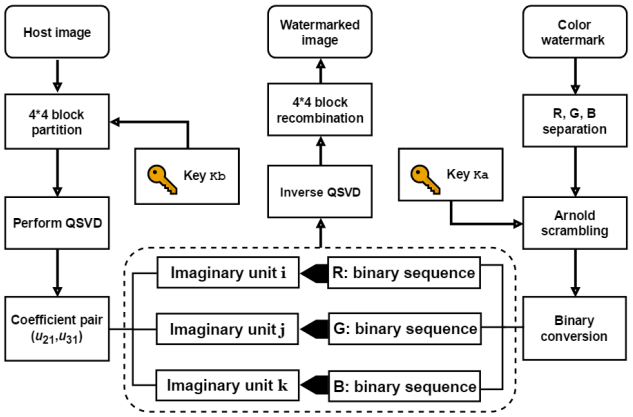

FIGURE 1. Diagram of the watermark embedding process.

the value of $(u_{21}-u_{31})_{\mathbf{i/j/k}}$ should be positive and its magnitude is greater than a threshold T. When these two conditions are violated, the elements of $(u_{21})_{\mathbf{i/j/k}}$ and $(u_{31})_{\mathbf{i/j/k}}$ should be modified as $(u_{21}^{\star})_{\mathbf{i/j/k}}$ and $(u_{31}^{\star})_{\mathbf{i/j/k}}$, respectively, based on the following rules in (IV-3)-(IV-4) to embed the watermark w_p and get the modified block $U_s^{\star}$,

$$if\, w_p = 1, \begin{cases} (u_{21}^{\star})_{\mathbf{i/j/k}} = sign((u_{21})_{\mathbf{i/j/k}}) \times (u_{avg} + \frac{T}{2}) \\ (u_{31}^{\star})_{\mathbf{i/j/k}} = sign((u_{31})_{\mathbf{i/j/k}}) \times (u_{avg} - \frac{T}{2}) \end{cases} \tag{IV-3}$$

$$if\, w_p = 0, \begin{cases} (u_{21}^{\star})_{\mathbf{i/j/k}} = sign((u_{21})_{\mathbf{i/j/k}}) \times (u_{avg} - \frac{T}{2}) \\ (u_{31}^{\star})_{\mathbf{i/j/k}} = sign((u_{31})_{\mathbf{i/j/k}}) \times (u_{avg} + \frac{T}{2}) \end{cases} \tag{IV-4}$$

where w_p is the watermark information, $(x)_{\mathbf{i/j/k}}$ denotes an element on the imaginary parts $\mathbf{i}$ or $\mathbf{j}$ or $\mathbf{k}$ of the quaternion x, sign(x) is the sign of x, $abs(x)$ is the absolute value of x and $u_{avg} = (abs((u_{21})_{\mathbf{i/j/k}}) + abs((u_{31})_{\mathbf{i/j/k}}))/2$.

Step 5: Obtaining the watermarked image block by

$$H_s^{\star} = U_s^{\star}\Sigma_s V_s^{*}. \tag{IV-5}$$

Step 6: Repeating Steps 3-5 by the private key `Kb` until all watermark information is embedded in the host image.

Step 7: Recombining all 4×4 watermarked blocks $H_s^{\star}$ to obtain the watermarked image $H^{\star}$.

B. WATERMARK EXTRACTION

Watermark extraction is the inverse operation of embedding mechanism. The watermark extraction procedure belongs to blind extraction method, that is, the original host image and watermark image are not needed in the procedure. The extraction details are described below.

Step 1: Obtaining the watermarked image. The watermarked image $H^{\star} = H_0^{\star} + H_1^{\star}\mathbf{i} + H_2^{\star}\mathbf{j} + H_3^{\star}\mathbf{k}$ is not a pure quaternion matrix. We set the real part H_0 of $H^{\star}$ to the same size zero matrix, then assume $H^{\star} = H_1^{\star}\mathbf{i} + H_2^{\star}\mathbf{j} + H_3^{\star}\mathbf{k}$ as a suspicious image with embedded watermark information.

Step 2: Obtaining the watermarked image block. The watermarked image $H^{\star}$ is partitioned into non-overlapping watermarked blocks of size 4×4 pixels. Then, we use a random coordinate sequence with the private key `Kb` to select the watermarked block $H_s^{\star}$.

Step 3: Applying Algorithm 1 to the watermarked block $H_s^{\star}$ and getting the matrices $U_s^{\star}$, $\Sigma_s^{\star}$, $V_s^{\star}$.

Step 4: Using (IV-6) and (IV-7) to extract the watermark information $w_p^{\star}$

$$\begin{cases} diff_{\mathbf{i}} = (u_{21} - u_{31})_{\mathbf{i}}, \\ diff_{\mathbf{j}} = (u_{21} - u_{31})_{\mathbf{j}}, \\ diff_{\mathbf{k}} = (u_{21} - u_{31})_{\mathbf{k}}, \end{cases} \tag{IV-6}$$

$$w_p^{\star} = \begin{cases} 1, & if\ diff_{\mathbf{i/j/k}} \geq 0, \\ 0, & if\ diff_{\mathbf{i/j/k}} < 0. \end{cases} \tag{IV-7}$$

Step 5: Repeating Steps 3-4 by the private key `Kb` until all embedded image blocks have been performed. These extracted binary sequences $w_p^{\star}$ are partitioned into 8-bit groups and converted to a decimal format, then the inverse Arnold scrambling with the private key `Ka` is performed and the extracted watermark of each component is reconstructed.

Step 6: Reconstructing the final color watermark $W^{\star}$ from extracted watermarks of the three imaginary parts.

C. EVALUATION CRITERIA

Generally, the performance of the watermarking methods is investigated by measuring their invisibility, robustness and capacity etc. For the imperceptible feature, the traditional metric PSNR, as shown in (IV-8), is used to measure the similarity between the original color image $H \in \mathbb{H}^{m\times n}$ and the watermarked image $H^{\star} \in \mathbb{H}^{m\times n}$.

$$PSNR = 10 \times lg \frac{3 \times m \times n \times (1)^2}{\| H - H^{\star} \|_F^2} dB \tag{IV-8}$$

where 1 represents the maximum value of a pixel in a color channel, and m, n denoted the height and width of an image respectively. $\| H - H^{\star} \|_F^2 = tr((H - H^{\star})^H (H - H^{\star})) = \| (H - H^{\star})_c^R \|_F^2$. In general, a larger PSNR indicates the watermarked image more closely resembles the original host image, which means that the watermark more imperceptible.

In addition, the metric BER,

$$BER = \frac{b}{3 \times e \times f} \tag{IV-9}$$

where b is the number of incorrectly detected bits, $e \times f$ is the size of the original watermark, is used to measure the dissimilarity between the extracted watermark and the original watermark. Generally, a lower BER reveals that the extracted watermark resembles the original watermark more closely.

V. NUMERICAL EXPERIMENTS

In this section, several experiments are performed to verify the effectiveness when incorporating our proposed two notes for QSVD-based watermarking scheme. Six 512×512 color

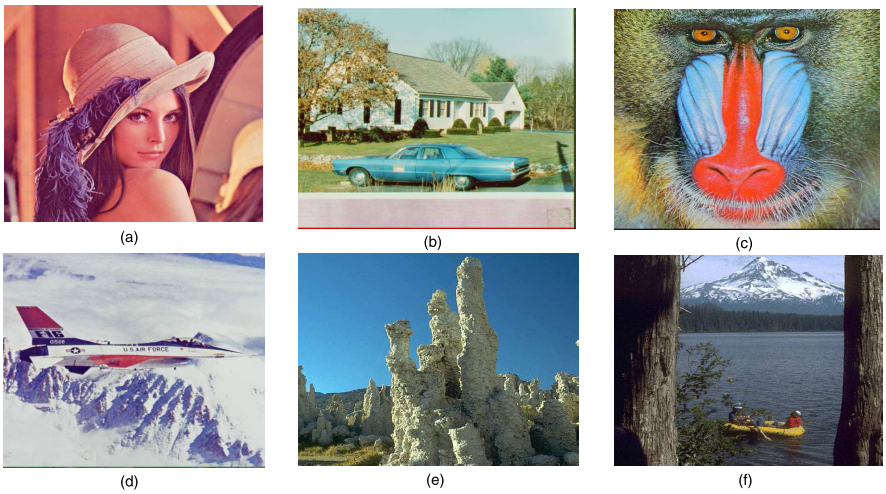

FIGURE 2. The original host image: (a) Lena, (b) House, (c) Baboon, (d) Avion, (e) Monolake, (f) Lostlake.

FIGURE 3. The original watermark image: peppers.

images in CVG-UGR image [45] database were used as host images as shown in Fig. 2. A color images is selected as original color watermark which was scaled to 32×32, as shown in Fig. 3. All these experiments were performed on an Intel(R) Core(TM) 64×64 Corei7-8750H @ 2.20GHz/8.00GB computer using MATLAB R2017b.

A. INVISIBILITY TEST

In order to evaluate the invisibility of the watermark, a comprehensive test of threshold T on the interval [0.002, 0.04] is carried out as shown in Fig. 5, and the watermarked color images and their PSNR values are specified in Fig. 4 when threshold $T = 0.022$. As can be seen from Figs. 4-5, the proposed method has a good watermark invisibility. The PSNR values are all greater than 30dB in the interval, which meets the requirements of literature [46]: if the PSNR values $\geq$ 28dB, then the visual quality of the image is unnoticeable. Without being attacked, the BER values for all watermarked images are close to zero, which means the original watermark can be recovered completely. Moreover, it can be concluded that there are slight differences between different images.

B. ROBUSTNESS TEST

In order to verify the robustness of the proposed method, when the watermarked image is attacked, the BER value of the extracted watermark should be less than 0.3, so as to ensure the visual quality of the extracted watermark [47].

1) COMPARISON OF THE PERFORMANCES OF SIMILAR SCHEMES

The proposed method is compared with similar methods in [21] and [22]. The blind dual-color watermarking scheme based on SVD [21] can ensure invisibility and strong robustness for some common attacks and geometric attacks. Reference [22] is the result of the method of [21] using V matrix compensation. This method increases the PSNR value of the watermarked image at a certain level. Considering the differences in the robustness and invisibility of different images, it is difficult to determine an optimal threshold to some extent. Therefore, a series of robustness tests are also performed at appropriate intervals [0.002, 0.04].

To highlight the robustness of the proposed method, different strengths of several different attacks are tested with images Lostlake and Lena, where the image Lena was tested and verified as a different image. Figs. 6-7 plot the variation of the BER values of the three methods within the set threshold interval. Fig. 8(a)-(n) visually show the reconstructed watermark image extracted from the watermarked image Lostlake at $T = 0.04$ under different attacks with different strengths. From Figs. 6-7 and Fig. 8(a)-(n), it can be seen that the proposed watermarking method has strong robustness against some common attacks, including JPEG compression, scaling, motion blur, Gaussian noise, speckle noise, contrast adjustment, cropping and histogram equalization. With the increase of threshold T, the BER values of the proposed scheme shows a significant downward trend, which means that the proposed method has strong robustness to cope with large modifications. We also find that the BER values of [21] is always lower than that of [22], as discussed in Section III-B, which verifies that the compensation scheme is equivalent to an additional watermark attack that makes the visual quality

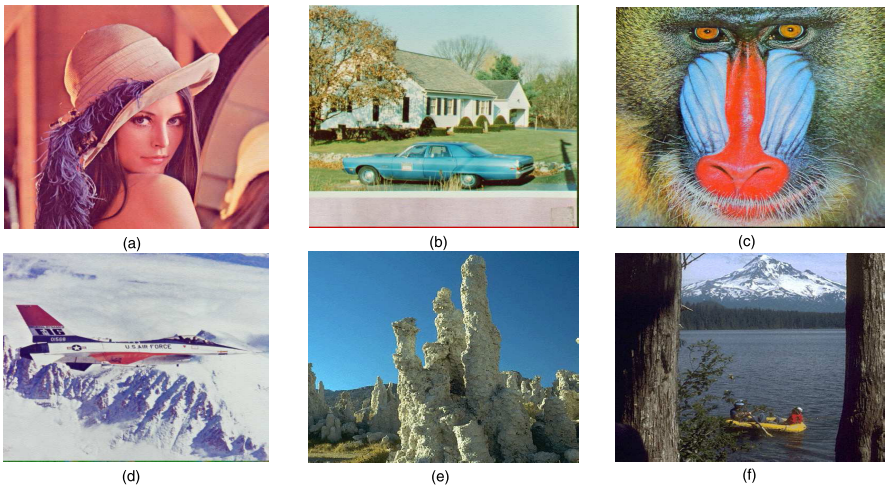

FIGURE 4. The watermarked image: (a) PSNR = 38.4640dB, (b) PSNR = 36.0873dB, (c) PSNR = 33.7715dB, (d) PSNR = 35.8859dB, (e) PSNR = 37.1872dB, (f) PSNR = 38.1892dB.

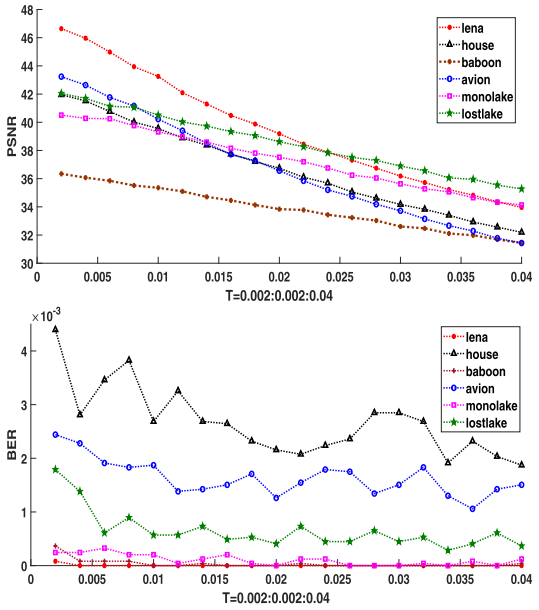

FIGURE 5. PSNR values of six color watermarked images and their BER values for watermarks extracted without any attack.

of the extracted watermark worse. Table 3 numerically lists the BER results compared to the methods in [21] and [22] when $T = 0.04$. As can be seen in Table 3, all the tested images and mentioned attacks in this paper are considered, and it also comprehensively shows that the proposed method has a stronger robustness than the methods of [21] and [22].

2) COMPARISON OF THE PERFORMANCES OF DIFFERENT SCHEMES

In order to further prove the robustness of the proposed method, the proposed method is also compared with two new blind color watermarking algorithms proposed in [23], [24]. The blind color watermarking algorithm based on Hessenberg matrix [23] uses the largest element in the Hessenberg matrix to embed the watermark through quantization modulation, which is very robust to JPEG compression and scaling attacks. The blind color watermarking algorithm based on LU decomposition [24] uses the strong correlation between some elements in the lower triangular matrix for watermark embedding, which can resist some common attacks. In [23], [24], a 32×32 color image was selected as the original watermark, and multiple 512×512 color images were tested as host images. Therefore, they are also dual-color watermarking, and the same embedding rate used for comparison is also fair. Considering that the robustness and invisibility are in conflict, and the differences between the various watermark embedding schemes, all experiments control the approximate PSNR value of each watermarked image (i.e., the watermarked image Lena $\approx$ 34dB, House $\approx$ 32dB, Baboon $\approx$ 32dB, Monolake $\approx$ 34dB, Avion $\approx$ 32dB, Lostlake $\approx$ 35dB). Therefore, the threshold of the embedding scheme in [23] in this paper is set to $T_1 = 0.28$, the threshold of the embedding scheme in [24] is set to $T_2 = 0.08$, and the threshold of our proposed scheme is set to $T = 0.04$. In the comparison experiments, the results are obtained by averaging the BER of 20 tests for each image. The results of comparison between the proposed scheme and those presented in references [23], [24] are listed in Table 4. The overall performance of the proposed scheme is superior to that of other different schemes. The main forms of geometric attacks include cropping, scaling, and common attacks such as noise, JPEG compression, filtering, contrast, and histogram equalization. The results show that the proposed scheme delivers significantly better performance than schemes [23], [24] under various attacks.

The results of the four aforementioned comparisons indicate that the scheme proposed in this paper is highly robust and superior to other schemes mentioned above.

C. THE SECURITY OF THE PROPOSED METHOD

In the proposed method, in order to make the selection of the watermark more universal and enhance the security of the

TABLE 3. Comparison of the robustness (BER) between the proposed scheme and similar watermarking schemes [21], [22] when the threshold $T = 0.04$.

Attack	Image	Proposed scheme	Scheme [21]	Scheme [22]	Image	Proposed scheme	Scheme [21]	Scheme [22]
JPEG40		0.1217	0.2837	0.2917		0.1125	0.2399	0.2453
JPEG60		0.0463	0.1784	0.1808		0.0408	0.1372	0.1468
JPEG80		0.0048	0.0646	0.0656		0.0099	0.0352	0.0400
Scaling0.5		0.0924	0.1713	0.1744		0.1777	0.2344	0.2367
Scaling2		0.0019	0.0169	0.0196		0.0146	0.0417	0.0452
Scaling4		0.0017	0.0157	0.0175		0.0142	0.0390	0.0426
Motion blur(4,4)		0.0006	0.0108	0.0117		0.0061	0.0193	0.0221
Motion blur(6,6)		0.0066	0.0302	0.0320		0.0261	0.0621	0.0654
Motion blur(9,9)		0.0280	0.0733	0.0753		0.0821	0.1372	0.1403
Gaussian noise0.01	Lena	0.1622	0.2869	0.2897	House	0.1238	0.2373	0.2415
Gaussian noise0.03		0.2827	0.3713	0.3748		0.2494	0.3374	0.3403
Speckle noise0.01		0.0330	0.1313	0.1378		0.0302	0.1283	0.1319
Speckle noise0.03		0.1237	0.2608	0.2655		0.1375	0.2530	0.2620
Speckle noise0.05		0.1784	0.3102	0.3128		0.2004	0.3080	0.3105
Cropping10%		0.0466	0.0466	0.0466		0.0484	0.0484	0.0484
Cropping50%		0.2366	0.2366	0.2366		0.2355	0.2355	0.2355
Brightening contrast(0.4,1)		0	0.0001	0.0002		0.0022	0.0005	0.0005
Darkening contrast(0,0.6)		0	0	0		0.0020	0.0011	0.0011
Histogram equalization		0.0099	0.0120	0.0127		0.0178	0.0107	0.0113
JPEG40		0.1278	0.2539	0.2582		0.0630	0.1783	0.1797
JPEG60		0.0487	0.1543	0.1622		0.0154	0.0802	0.0854
JPEG80		0.0046	0.0421	0.0397		0.0024	0.0161	0.0138
Scaling0.5		0.2722	0.3404	0.3431		0.1028	0.1448	0.1466
Scaling2		0.0280	0.0851	0.0925		0.0093	0.0216	0.0233
Scaling4		0.0262	0.0814	0.0893		0.0088	0.0203	0.0217
Motion blur(4,4)		0.0200	0.0684	0.0756		0.0031	0.0082	0.0093
Motion blur(6,6)		0.0651	0.1339	0.1402		0.0127	0.0306	0.0323
Motion blur(9,9)		0.1433	0.2195	0.2243		0.0428	0.0761	0.0781
Gaussian noise0.01	Baboon	0.1484	0.2511	0.2532	Avion	0.0881	0.2093	0.2122
Gaussian noise0.03		0.2671	0.3396	0.3416		0.2170	0.3202	0.3242
Speckle noise0.01		0.0288	0.1128	0.1203		0.0279	0.1303	0.1350
Speckle noise0.03		0.1178	0.2257	0.2327		0.1447	0.2693	0.2734
Speckle noise0.05		0.1709	0.2717	0.2763		0.2199	0.3231	0.3252
Cropping10%		0.0462	0.0462	0.0462		0.0489	0.0489	0.0489
Cropping50%		0.2351	0.2351	0.2351		0.2359	0.2361	0.2361
Brightening contrast(0.4,1)		0	0.0003	0.0003		0.0013	0.0001	0.0001
Darkening contrast(0,0.6)		0	0	0		0.0015	0.0013	0.0013
Histogram equalization		0.0086	0.0139	0.0154		0.0235	0.0105	0.0109
JPEG40		0.1663	0.3166	0.3189		0.2719	0.3615	0.3662
JPEG60		0.0749	0.2050	0.2130		0.1809	0.2749	0.2850
JPEG80		0.0117	0.0772	0.0789		0.0791	0.1498	0.1516
Scaling0.5		0.1675	0.2293	0.2316		0.2851	0.3540	0.3565
Scaling2		0.0088	0.0363	0.0397		0.0139	0.0634	0.0698
Scaling4		0.0078	0.0339	0.0379		0.0122	0.0598	0.0666
Motion blur(4,4)		0.0091	0.0338	0.0373		0.0129	0.0481	0.0531
Motion blur(6,6)		0.0320	0.0712	0.0746		0.0464	0.1116	0.1171
Motion blur(9,9)		0.0820	0.1365	0.1396		0.1349	0.2184	0.2236
Gaussian noise0.01	Monolake	0.2008	0.3042	0.3091	Lostlake	0.2699	0.3418	0.3426
Gaussian noise0.03		0.3091	0.3804	0.3838		0.3549	0.4059	0.4074
Speckle noise0.01		0.0324	0.1225	0.1307		0.0336	0.1241	0.1293
Speckle noise0.03		0.1228	0.2447	0.2500		0.1312	0.2401	0.2448
Speckle noise0.05		0.1767	0.2937	0.2973		0.1897	0.2888	0.2900
Cropping10%		0.0469	0.0469	0.0469		0.0470	0.0474	0.0474
Cropping50%		0.2343	0.2343	0.2343		0.2353	0.2356	0.2356
Brightening contrast(0.4,1)		0.0001	0.0017	0.0019		0.0008	0.0046	0.0052
Darkening contrast(0,0.6)		0	0.0005	0.0007		0.0005	0.0006	0.0006
Histogram equalization		0.0150	0.0220	0.0227		0.0077	0.0200	0.0208

TABLE 4. Comparison of the robustness (BER) between the proposed scheme and schemes [23], [24].

Attack	Image	Proposed scheme $T = 0.04$	Scheme [23] $T_1 = 0.28$	Scheme [24] $T_2 = 0.08$	Image	Proposed scheme $T = 0.04$	Scheme [23] $T_1 = 0.28$	Scheme [24] $T_2 = 0.08$
JPEG40		0.1217	0.0228	0.2769		0.1125	0.0256	0.2336
JPEG60		0.0463	0.0078	0.2322		0.0408	0.0101	0.1953
JPEG80		0.0048	0.0048	0.1866		0.0099	0.0046	0.1509
Scaling0.5		0.0924	0.0784	0.2570		0.1777	0.1215	0.2969
Scaling2		0.0019	0.0024	0.0719		0.0146	0.0042	0.0796
Scaling4		0.0017	0.0020	0.0699		0.0142	0.0041	0.0801
Motion blur(4,4)		0.0006	0.1193	0.1689		0.0061	0.1528	0.1538
Motion blur(6,6)		0.0066	0.3033	0.1895		0.0261	0.3336	0.1785
Motion blur(9,9)		0.0280	0.4152	0.2122		0.0821	0.4288	0.2231
Gaussian noise0.01	Lena	0.1622	0.4688	0.3602	House	0.1238	0.4640	0.3267
Gaussian noise0.03		0.2827	0.4971	0.4192		0.2494	0.4989	0.3952
Speckle noise0.01		0.0330	0.1936	0.2464		0.0302	0.2723	0.2489
Speckle noise0.03		0.1237	0.3712	0.3375		0.1375	0.4330	0.3317
Speckle noise0.05		0.1784	0.4249	0.3702		0.2004	0.4624	0.3682
Cropping10%		0.0466	0.0488	0.0456		0.0484	0.0484	0.0475
Cropping50%		0.2366	0.2404	0.2345		0.2355	0.2323	0.2339
Brightening contrast(0.4,1)		0	0.4145	0.0022		0.0022	0.3540	0.0033
Darkening contrast(0,0.6)		0	0.6059	0.0013		0.0020	0.6294	0.0035
Histogram equalization		0.0099	0.6339	0.0546		0.0178	0.5686	0.0435
JPEG40		0.1278	0.1023	0.2405		0.0630	0.0170	0.2268
JPEG60		0.0487	0.0579	0.1942		0.0154	0.0040	0.2008
JPEG80		0.0046	0.0162	0.1223		0.0024	0.0026	0.1700
Scaling0.5		0.2722	0.2626	0.3502		0.1028	0.0771	0.2510
Scaling2		0.0280	0.0356	0.0787		0.0093	0.0023	0.0845
Scaling4		0.0262	0.0312	0.0736		0.0088	0.0022	0.0832
Motion blur(4,4)		0.0200	0.2667	0.1912		0.0031	0.1017	0.1600
Motion blur(6,6)		0.0651	0.4126	0.2078		0.0127	0.2834	0.1777
Motion blur(9,9)		0.1433	0.4752	0.2177		0.0428	0.3993	0.2055
Gaussian noise0.01	Baboon	0.1484	0.4806	0.2875	Avion	0.0881	0.4618	0.3262
Gaussian noise0.03		0.2671	0.5020	0.3693		0.2170	0.4993	0.3909
Speckle noise0.01		0.0288	0.2225	0.1644		0.0279	0.3337	0.2754
Speckle noise0.03		0.1178	0.4000	0.2591		0.1447	0.4736	0.3546
Speckle noise0.05		0.1709	0.4503	0.3003		0.2199	0.4877	0.3839
Cropping10%		0.0462	0.0484	0.0473		0.0489	0.0472	0.0470
Cropping50%		0.2351	0.2360	0.2365		0.2359	0.2346	0.2380
Brightening contrast(0.4,1)		0	0.4375	0.0008		0.0013	0.2898	0.0030
Darkening contrast(0,0.6)		0	0.6030	0.0004		0.0015	0.7593	0.0026
Histogram equalization		0.0086	0.4403	0.0250		0.0235	0.5484	0.0345
JPEG40		0.1663	0.0970	0.2928		0.2719	0.0691	0.3302
JPEG60		0.0749	0.0655	0.2443		0.1809	0.0442	0.2781
JPEG80		0.0117	0.0405	0.1872		0.0791	0.0317	0.2080
Scaling0.5		0.1675	0.1766	0.3240		0.2851	0.1776	0.3772
Scaling2		0.0088	0.0494	0.1497		0.0139	0.0227	0.1466
Scaling4		0.0078	0.0488	0.1515		0.0122	0.0207	0.1447
Motion blur(4,4)		0.0091	0.1918	0.2159		0.0129	0.2105	0.2009
Motion blur(6,6)		0.0320	0.3350	0.2346		0.0464	0.3580	0.2295
Motion blur(9,9)		0.0820	0.4212	0.2620		0.1349	0.4314	0.2727
Gaussian noise0.01	Monolake	0.2008	0.4798	0.3611	Lostlake	0.2699	0.4861	0.3763
Gaussian noise0.03		0.3091	0.4966	0.4122		0.3549	0.5038	0.4300
Speckle noise0.01		0.0324	0.1645	0.2245		0.0336	0.1185	0.2051
Speckle noise0.03		0.1228	0.3359	0.3094		0.1312	0.2570	0.2955
Speckle noise0.05		0.1767	0.4078	0.3419		0.1897	0.3262	0.3339
Cropping10%		0.0469	0.0606	0.0455		0.0470	0.0554	0.0461
Cropping50%		0.2343	0.2432	0.2349		0.2353	0.2387	0.2361
Brightening contrast(0.4,1)		0.0001	0.4224	0.0051		0.0008	0.3904	0.0052
Darkening contrast(0,0.6)		0	0.5900	0.0020		0.0005	0.5891	0.0025
Histogram equalization		0.0150	0.4021	0.0132		0.0077	0.4926	0.0210

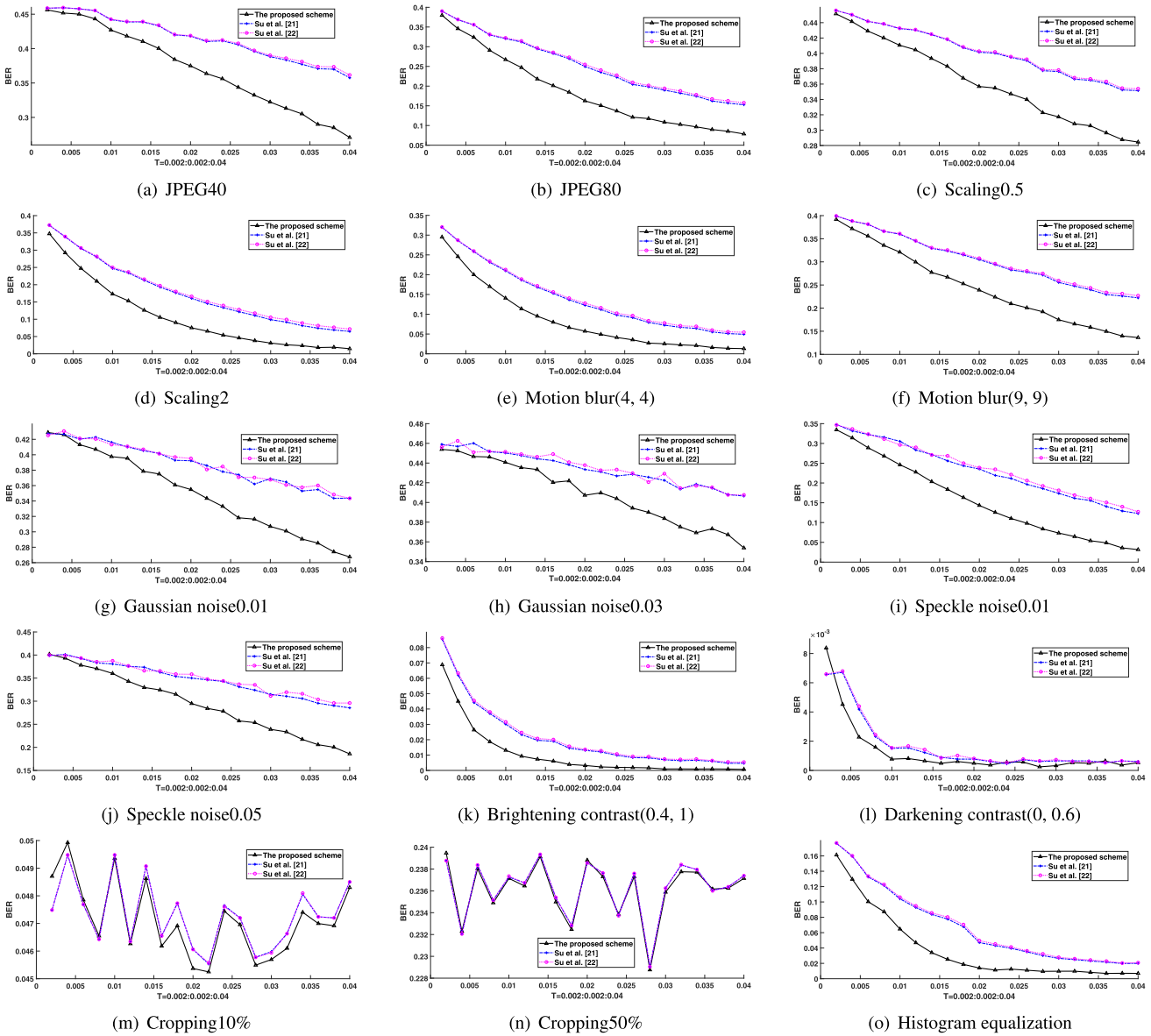

FIGURE 6. Robustness comparison between our method and two methods of Su *et al.* [21] and Su *et al.* [22] on watermarked image Lostlake with different attacks.

watermarking scheme, each channel of the color watermark is scrambled by Arnold scrambling with the private key `Ka` as shown in Fig. 8 (o)-(r). On the other hand, random and non-overlapping embedded blocks are selected by random coordinate sequence with the private key `Kb`. Therefore, compared with the schemes in [21] and [22], the proposed scheme is almost impossible to reconstruct the correct watermark without the correct key.

D. THE CAPACITY OF THE PROPOSED METHOD

The watermark capacity is a key indicator used to measure the performance of a watermarking scheme [48], [49]. In this paper, the maximum capacity is equal to three times the number of 4×4 host image blocks, which is determined by the three highly correlated statistical features proposed based on QSVD. As shown in Fig. 1, each embedded 4×4 image block carries three bits of information. Therefore, for a 512×512 host image, the maximum payload capacity based on QSVD is $128\times128\times3$. In addition, the watermark capacity is also analyzed by the embedding rate. The embedding rate expressed in bits per pixel (bpp) is a pure payload (i.e., the total number of embedded bits minus the total amount of all overhead information) [50]. As shown in Fig. 5, the actual payload is limited by the distortion of the watermarked image. For the sake of fairness, in all experiments, the embedded watermark is set to a 32×32 color image and the host image is a 512×512 color image, so the embedding rate is $(32\times32\times8\times3)/(512\times512\times3)=0.03125$ (bpp). It is obvious that the proposed algorithm has a high level of capacity.

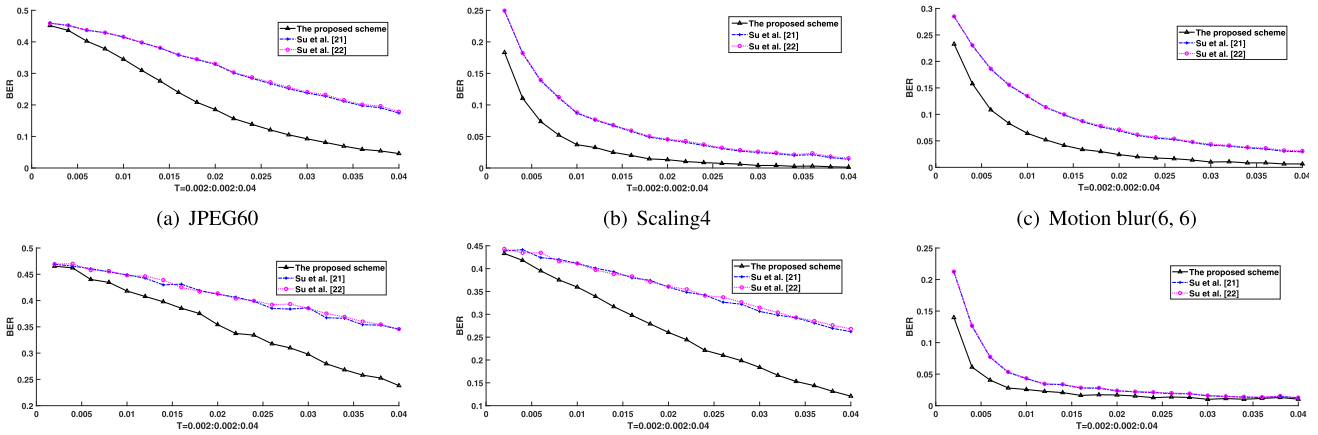

(a) JPEG60 (b) Scaling4 (c) Motion blur(6, 6)

(d) Gaussian noise0.02 (e) Speckle0.03 (f) Histogram equalization

FIGURE 7. Robustness comparison between our method and two methods of Su *et al.* [21] and Su *et al.* [22] on watermarked image Lena with different attacks.

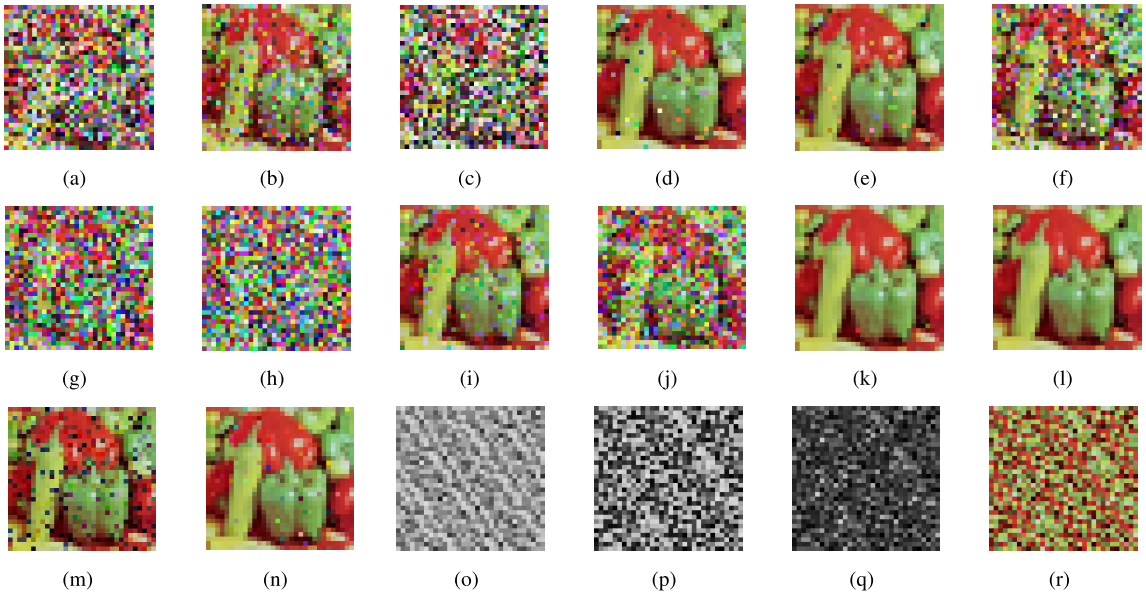

(a) (b) (c) (d) (e) (f)

(g) (h) (i) (j) (k) (l)

(m) (n) (o) (p) (q) (r)

FIGURE 8. Extracted watermarks after different attacks: (a) JPEG40, (b) JPEG80, (c) scaling0.5, (d) scaling2, (e) motion blur [4,4], (f) motion blur [9,9], (g) Gaussian noise0.01, (h) Gaussian noise0.03, (i) speckle noise0.01, (j) speckle noise0.05, (k) brightening contrast [0.4,1], (l) darkening contrast [0,0.6], (m) cropping10%, (n) histogram equalization. Scrambled original watermarks: (o) R component, (p) G component, (q) B component, (r) scrambled watermark.

In summary, the proposed algorithm not only meets transparency, but also has stronger robustness, better security, high information capacity, and low computational complexity.

VI. CONCLUSION

In this paper, we have proposed a robust dual-color watermarking based on QSVD. Firstly, a fast algebraic structure-preserving algorithm is presented to implement QSVD. Secondly, according to the algebraic feature of QSVD, the color watermark is embedded into a color host image by modifying the relationship between the second row element and the third row element of the first column of each coefficient matrix of the three imaginary parts in the U matrix. Experimental results and theoretical analysis show that the proposed scheme successfully makes the watermark imperceptible and robust against various geometric attacks and signal processing operations, and also verify the shortcomings of SVD-based compensation scheme. Compared with the watermarking schemes listed in this paper, the new proposed scheme has better performance to protect the copyright of color images that will be transmitted over the Internet. The future work mainly focuses on the parallelization of QSVD of each image block to improve the efficiency of the entire watermarking scheme. We also plan to apply the proposed scheme to new research advances such as multi-image copyright protection [51] and image tamper detection [52], [53].

REFERENCES

[1] D. Li, X. Che, W. Luo, Y. Hu, Y. Wang, Z. Yu, and L. Yuan, "Digital watermarking scheme for colour remote sensing image based on quaternion wavelet transform and tensor decomposition," *Math. Methods Appl. Sci.*, vol. 42, no. 14, pp. 4664–4678, Sep. 2019.

[2] J. Serra-Ruiz, A. Qureshi, and D. Megías, "Entropy-based semi-fragile watermarking of remote sensing images in the wavelet domain," *Entropy*, vol. 21, no. 9, p. 847, Aug. 2019.

[3] N. Dey, S. Samanta, S. Chakraborty, A. Das, S. S. Chaudhuri, and J. S. Suri, "Firefly algorithm for optimization of scaling factors during embedding of manifold medical information: An application in ophthalmology imaging," *J. Med. Imag. Health Inf.*, vol. 4, no. 3, pp. 384–394, Jun. 2014.

[4] N. Dey, G. Dey, S. Chakraborty, and S. S. Chaudhuri, "Feature analysis of blind watermarked electromyogram signal in wireless telemonitoring," in *Concepts and Trends in Healthcare Information Systems*. Cham, Switzerland: Springer, 2014, pp. 205–229.

[5] N. Dey, A. Roy, A. Das, and S. S. Chaudhuri, "Stationary wavelet transformation based self-recovery of blind-watermark from electrocardiogram signal in wireless telecardiology," in *Proc. Int. Conf. Secur. Comput. Netw. Distrib. Syst.*, Berlin, Germany, 2012, pp. 347–357.

[6] S. Borra, N. Dey, A. S. Ashour, and F. Shi, "Digital image watermarking tools: State-of-the-art," in *Proc. 2nd Int. Conf. Inform. Tech. Intell. Trans. Sys. (ITITS)*, Xian, China, 2017, pp. 450–459.

[7] S. B. B. Ahmadi, G. Zhang, and S. Wei, "Robust and hybrid SVD-based image watermarking schemes:: A survey," *Multimedia Tools Appl.*, vol. 79, nos. 1–2, pp. 1075–1117, Jan. 2020, doi: 10.1007/s11042-019-08197-6.

[8] N. Dey, P. Das, A. B. Roy, A. Das, and S. S. Chaudhuri, "DWT-DCT-SVD based intravascular ultrasound video watermarking," in *Proc. World Congr. Inf. Commun. Technol.*, Oct. 2012, pp. 224–229.

[9] N. Dey, S. Biswas, A. Roy, A. Das, and S. S. Chowdhuri, "Analysis of photoplethysmographic signals modified by reversible watermarking technique using prediction-error in wireless telecardiology," in *Proc. 47th Annu. Nat. Conv. CSI Int. Conf. Intell. Infrastruct.*, New Delhi, India, 2012, pp. 1–6.

[10] N. Dey, A. S. Ashour, S. Chakraborty, S. Banerjee, E. Gospodinova, M. Gospodinov, and A. Hassanien, "Watermarking in biomedical signal processing," in *Intelligent Techniques in Signal Processing for Multimedia Security*. Cham, Switzerland: Springer, 2017, pp. 345–369.

[11] C.-P. Wang, X.-Y. Wang, X.-J. Chen, and C. Zhang, "Robust zero-watermarking algorithm based on polar complex exponential transform and logistic mapping," *Multimedia Tools Appl.*, vol. 76, no. 24, pp. 26355–26376, Dec. 2017.

[12] W. Chun-peng, W. Xing-yuan, and X. Zhi-qiu, "Geometrically invariant image watermarking based on fast Radial Harmonic Fourier Moments," *Signal Process., Image Commun.*, vol. 45, pp. 10–23, Jul. 2016.

[13] C. Chang, P. Tsai, and C. Lin, "SVD-based digital image watermarking scheme," *Pattern Recogn. Lett.*, vol. 26, no. 10, pp. 1577–1586, 2005.

[14] K.-L. Chung, W.-N. Yang, Y.-H. Huang, S.-T. Wu, and Y.-C. Hsu, "On SVD-based watermarking algorithm," *Appl. Math. Comput.*, vol. 188, no. 1, pp. 54–57, 2007.

[15] M.-Q. Fan, H.-X. Wang, and S.-K. Li, "Restudy on SVD-based watermarking scheme," *Appl. Mathematics Comput.*, vol. 203, no. 2, pp. 926–930, Sep. 2008.

[16] J. Liu, J. Huang, Y. Luo, L. Cao, S. Yang, D. Wei, and R. Zhou, "An optimized image watermarking method based on HD and SVD in DWT domain," *IEEE Access*, vol. 7, pp. 80849–80860, 2019.

[17] M. Kutter and F. Bossen, "Digital signature of color images using amplitude modulation," *J. Electron. Imag.*, vol. 7, no. 2, pp. 326–332 1998.

[18] B. Abdelhamid and L. Lamri, "New images watermarking scheme based on singular value decomposition," *J. Inf. Hiding Multimedia Signal Process.*, vol. 4, no. 1, pp. 1–10, 2013.

[19] Q. Su, Y. Niu, G. Wang, S. Jia, and J. Yue, "Color image blind watermarking scheme based on QR decomposition," *Signal Process.*, vol. 94, pp. 219–235, Jan. 2014.

[20] M. Natarajan and Y. Govindarajan, "A study of DWT-SVD based multiple watermarking scheme for medical Images," *Int. J. Netw. Secur.*, vol. 17, no. 5, pp. 558–568, 2015.

[21] Q. Su, Y. Niu, H. Zou, and X. Liu, "A blind dual color images watermarking based on singular value decomposition," *Appl. Math. Comput.*, vol. 219, no. 16, pp. 8455–8466, Apr. 2013.

[22] Q. Su, Y. Niu, Y. Zhao, S. Pang, and X. Liu, "A dual color images watermarking scheme based on the optimized compensation of singular value decomposition," *AEU-Int. J. Electron. Commun.*, vol. 67, no. 8, pp. 652–664, Aug. 2013.

[23] Q. Su and B. Chen, "A novel blind color image watermarking using upper Hessenberg matrix," *AEU-Int. J. Electron. Commun.*, vol. 78, pp. 64–71, Aug. 2017.

[24] Q. Su, G. Wang, X. Zhang, G. Lv, and B. Chen, "A new algorithm of blind color image watermarking based on LU decomposition," *Multidimensional Syst. Signal Process.*, vol. 29, no. 3, pp. 1055–1074, Jul. 2018.

[25] Y. Li, M. Wei, F. Zhang, and J. Zhao, "A new double color image watermarking algorithm based on the SVD and arnold scrambling," *J. Appl. Math.*, vol. 2016, pp. 1–9, Jan. 2016.

[26] C.-P. Wang, X.-Y. Wang, Z.-Q. Xia, C. Zhang, and X.-J. Chen, "Geometrically resilient color image zero-watermarking algorithm based on quaternion Exponent moments," *J. Vis. Commun. Image Represent.*, vol. 41, pp. 247–259, Nov. 2016.

[27] C. Wang, X. Wang, C. Zhang, and Z. Xia, "Geometric correction based color image watermarking using fuzzy least squares support vector machine and Bessel K form distribution," *Signal Process.*, vol. 134, pp. 197–208, May 2017.

[28] Z. Xia, X. Wang, W. Zhou, R. Li, C. Wang, and C. Zhang, "Color medical image lossless watermarking using chaotic system and accurate quaternion polar harmonic transforms," *Signal Process.*, vol. 157, pp. 108–118, Apr. 2019.

[29] C. Wang, X. Wang, Z. Xia, and C. Zhang, "Ternary radial harmonic Fourier moments based robust stereo image zero-watermarking algorithm," *Inf. Sci.*, vol. 470, pp. 109–120, Jan. 2019.

[30] C. Wang, X. Wang, Y. Li, Z. Xia, and C. Zhang, "Quaternion polar harmonic Fourier moments for color images," *Inf. Sci.*, vol. 450, pp. 141–156, Jun. 2018.

[31] Z. Xia, X. Wang, M. Wang, S. Unar, C. Wang, Y. Liu, and X. Li, "Geometrically invariant color medical image null-watermarking based on precise quaternion polar harmonic Fourier moments," *IEEE Access*, vol. 7, pp. 122544–122560, 2019.

[32] S. Chakraborty, S. Chatterjee, N. Dey, A. S. Ashour, and A. E. Hassanien, "Comparative approach between singular value decomposition and randomized singular value decomposition-based watermarking," in *Proc. Intell. Tech. signal Process. Multimedia Secur.*, 2017, pp. 133–149.

[33] P. Bao and X. Ma, "Image adaptive watermarking using wavelet domain singular value decomposition," *IEEE Trans. Circuits Syst. Video Technol.*, vol. 15, no. 1, pp. 96–102, Jan. 2005.

[34] C.-S. Chang and J.-J. Shen, "Features classification forest: A novel development that is adaptable to robust blind watermarking techniques," *IEEE Trans. Image Process.*, vol. 26, no. 8, pp. 3921–3935, Aug. 2017.

[35] H. Zhang, C. Wang, and X. Zhou, "A robust image watermarking scheme based on SVD in the spatial domain," *Future Internet*, vol. 9, no. 3, p. 45, Aug. 2017.

[36] W. R. Hamilton, *The Mathematical Papers of Sir William Rowan Hamilton*. Cambridge, U.K.: Cambridge Univ. Press, 1967.

[37] G. H. Golub and C. F. Van Loan, *Matrix Computations*, 4th ed. Baltimore, MD, USA: The Johns Hopkins Univ. Press, 2013.

[38] S. J. Sangwine and N. Le Bihan. *Quaternion Toolbox for MATLAB*. [Online]. Available: http://qtfm.sourceforge.net/

[39] Z. Jia, M. Wei, and S. Ling, "A new structure-preserving method for quaternion Hermitian eigenvalue problems," *J. Comput. Appl. Math.*, vol. 239, pp. 12–24, Feb. 2013.

[40] Z. Jia, M. Wei, M.-X. Zhao, and Y. Chen, "A new real structure-preserving quaternion QR algorithm," *J. Comput. Appl. Math.*, vol. 343, pp. 26–48, Dec. 2018.

[41] Y. Li, M. Wei, F. Zhang, and J. Zhao, "Real structure-preserving algorithms of householder based transformations for quaternion matrices," *J. Comput. Appl. Math.*, vol. 305, pp. 82–91, Oct. 2016.

[42] Y. Li, M. Wei, F. Zhang, and J. Zhao, "A fast structure-preserving method for computing the singular value decomposition of quaternion matrices," *Appl. Math. Comput.*, vol. 235, pp. 157–167, May 2014.

[43] R.-R. Ma, Z.-G. Jia, and Z.-J. Bai, "A structure-preserving Jacobi algorithm for quaternion Hermitian eigenvalue problems," *Comput. Math. Appl.*, vol. 75, no. 3, pp. 809–820, Feb. 2018.

[44] Z. Jia, M. K. Ng, and G. Song, "Lanczos method for large-scale quaternion singular value decomposition," *Numer. Algorithms*, vol. 82, no. 2, pp. 699–717, 2019.

[45] Unversity of Granada. (Oct. 22, 2012). *Computer Vision Group. CVG-UGR Image Data Base*. [Online]. Available: http://decsai.ugr.es/cvg/dbimagenes/c512.php

[46] G. Bhatnagar, Q. J. Wu, and B. Raman, "A new robust adjustable logo watermarking scheme," *Comput. Secur.*, vol. 31, no. 1, pp. 40–58, Feb. 2012.

[47] F. Liu, L.-H. Ma, C. Liu, and Z.-M. Lu, "Optimal blind watermarking for color images based on the U matrix of quaternion singular value decomposition," *Multimedia Tools Appl.*, vol. 77, no. 18, pp. 23483–23500, Sep. 2018.
[48] S. Banerjee, S. Chakraborty, N. Dey, A. Kumar Pal, and R. Ray, "High payload watermarking using residue number system," *Int. J. Image, Graph. Signal Process.*, vol. 7, no. 3, pp. 1–8, Feb. 2015.
[49] A. Kumar Pal, P. Das, and N. Dey, "Odd-even embedding scheme based modified reversible watermarking technique using blueprint," 2013, *arXiv:1303.5972*. [Online]. Available: http://arxiv.org/abs/1303.5972
[50] H.-T. Wu and J. Huang, "Reversible image watermarking on prediction errors by efficient histogram modification," *Signal Process.*, vol. 92, no. 12, pp. 3000–3009, Dec. 2012.
[51] Z. Xia, X. Wang, X. Li, C. Wang, S. Unar, M. Wang, and T. Zhao, "Efficient copyright protection for three CT images based on quaternion polar harmonic Fourier moments," *Signal Process.*, vol. 164, pp. 368–379, Nov. 2019.
[52] L. Teng, X. Wang, and X. Wang, "Cryptanalysis and improvement of a chaotic system based fragile watermarking scheme," *AEU-Int. J. Electron. Commun.*, vol. 67, no. 6, pp. 540–547, Jun. 2013.
[53] I. A. Ansari, M. Pant, and C. W. Ahn, "SVD based fragile watermarking scheme for tamper localization and self-recovery," *Int. J. Mach. Learn. Cyber.*, vol. 7, no. 6, pp. 1225–1239, Dec. 2016.

YONG CHEN received the M.Sc. degree in mathematics from Jiangsu Normal University, Xuzhou, China, in 2018. He is currently pursuing the Ph.D. degree with the School of Mechatronic Engineering and Automation, Shanghai University, Shanghai, China. His research interests include numerical algebra and image processing.

ZHIGANG JIA received the Ph.D. degree in mathematics from East China Normal University, Shanghai, China, in 2009. He is currently a Professor of mathematics with the School of Mathematics and Statistics, Jiangsu Normal University, Xuzhou, China. His current research interests include numerical linear algebra, machine learning, eigenvalue theory and algorithms, quaternion matrix computations, color image recognition, and imaging science.

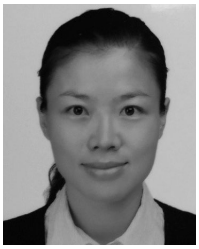

YAN PENG received the Ph.D. degree in pattern recognition and intelligent systems from the Shenyang Institute of Automation, Chinese Academy of Sciences, Shenyang, China, in 2009. She is currently a Professor with Shanghai University, Shanghai, China, as the Dean of the Research Institute of USV Engineering. Her current research interests include modeling and control of unmanned surface vehicles, field robotics, and locomotion systems.

YAXIN PENG (Member, IEEE) received the B.Sc. degree in mathematics from Anhui Normal University, Wuhu, China, in 2002, the M.Sc. degree in mathematics from East China Normal University (ECNU), Shanghai, China, in 2005, and the Ph.D. degree in mathematics from the É cole Normale Sup é rieure de Lyon, Lyon, France, and ECNU, in 2008. She is currently an Associate Professor with the Department of Mathematics, School of Science, Shanghai University, Shanghai. Her research interests include geometric variation, metric learning, point cloud, and image processing.